Case Studies in Thermal Engineering 38 (2022) 102310

Contents lists available at ScienceDirect

Case Studies in Thermal Engineering

journal homepage: www.elsevier.com/locate/csite

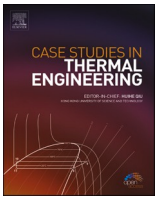

Comparison on the heat transfer performance and entropy analysis on miniature loop thermosyphon with screen mesh wick and metal foam

Stephen Manova [a,b], Lazarus Godson Asirvatham [a,b,*], Appadurai Anitha Angeline [c], Sheno Jerbin [a], Jefferson Raja Bose [a], Rajesh Nimmagadda [d], Russel Jayaseelan [a], Somchai Wongwises [e,f]

[a] Department of Mechanical Engineering, Karunya Institute of Technology and Sciences, Coimbatore, 641 114, Tamil Nadu, India
[b] Centre for Research in Material Science and Thermal Management (CRMS &TM), Karunya Institute of Technology and Sciences, Coimbatore, 641 114, Tamil Nadu, India
[c] Department of Robotics Engineering, Karunya Institute of Technology and Sciences, Coimbatore 641 114, Tamil Nadu, India
[d] Center for Advanced Energy Studies, Koneru Lakshmaiah Educational Foundation, Vaddeswaram, (A.P), India
[e] Department of Mechanical Engineering, Faculty of Engineering, King Mongkut's University of Technology Thonburi (KMUTT), Bangmod, Bangkok, 10140, Thailand
[f] National Science and Technology Development Agency (NSTDA), Pathum Thani, 12120, Thailand

ARTICLE INFO

Keywords:
Loop thermosyphon
Metal foams
DI water
Entropy
Copper screen wick

ABSTRACT

Comparison on the heat transfer performance (HTP) of copper screen mesh wick and metal foam inserted evaporator section of miniature loop thermosyphon is experimentally investigated. Porosity of both screen mesh wick and metal foams are fixed to be 63%. Experiments are conducted using DI water under vertical orientation for different heat loads (40 W–280 W) and filling ratios (FR = 20%, 30% and 40%). Results showed a decrease of 12.8% and 5.2% in thermal resistance and wall temperature respectively for the metal foam inserted evaporator. In addition 10.6% enhancement is noted for heat transfer coefficient at the evaporator region for 30% FR. Reduction of 4.6% in heat transfer irreversibility is also noted for metal foam inserted thermosyphon compared to screen mesh wick condition. Increase in interstitial heat transfer between the fibers of metal foam and larger pore size of metal foams resulted in higher permeability compared to screen mesh wick are responsible for the enhancement in the overall HTP of metal foam inserted thermosyphon. Based on the observed results, the use of metal foams inserted thermosyphon will be a better substitute for thermal management applications of electronic devices.

1. Introduction

The immense growth in the production of modern electronic devices resulted in continuous development of high end processors. The heat flux dissipation value reaches over 100 W/cm^2 and it is expected to be even higher in near future [1]. Reducing the dimension of electronic products simultaneously increases the heat generation rate of these processors which becomes undesirable for the

* Corresponding author. , , Department of Mechanical Engineering, Karunya Institute of Technology and Sciences, Coimbatore, 641 114, Tamil Nadu, India.
E-mail addresses: manovas@karunya.edu.in (S. Manova), godson@karunya.edu, godsonasirvatham@gmail.com (L. Godson Asirvatham), anithaangeline@karunya.edu (A.A. Angeline), shenojerbin@gmail.com (S. Jerbin), jefferson@karunya.edu (J.R. Bose), rajesh.mech335@gmail.com (R. Nimmagadda), seelan@karunya.edu (R. Jayaseelan), somchai.won@kmutt.ac.th (S. Wongwises).

https://doi.org/10.1016/j.csite.2022.102310
Received 28 June 2021; Received in revised form 11 July 2022; Accepted 18 July 2022
Available online 22 July 2022

manufacturing industries. Even though, the field of electronics has its foot print on miniaturization, an effective passive cooling technology for these high heat flux dissipating processing chips is deficient and became a pressing need [2–5]. Based on the survey of International Road of Semiconductors (ITRS 2010), these microprocessors are expected to dissipate an average heat flux ranging from 200 to 450 W/cm^2 by 2026 [6]. Moreover, the hot spots in these processors were predicted to be 6–10 times higher than the average power consumption. Therefore, a cooling system which is efficient that can satisfy the present electronic cooling requirements is very much essential and has become an active research in electronic industries [7–9].

Many researchers have acknowledged thermosyphon cooling technology as one of the best possible solutions to meet the present electronic cooling requirement. Particularly, loop thermosyphon are specially appraised in the open literatures due to its advantage of higher heat transport capability [10]. Also, the two-phase cooling technology with different transport lines of loop heat pipe increases its feasibility of installing in many cooling applications. In addition, research works on screen wicks [11], nanoparticle coating [12] and sintered wicks [13,14] are also investigated. The wick structure is considered to be an essential factor in loop heat pipes, as the capillary pressure is the driving mechanism for its effective operation. Generally, the HTP enhancement is achieved by the surface modification and capillary improvement made in the evaporator section of loop heat pipes [15,16]. Some of the most productive works on experimental investigations of loop heat pipe using screen wicks, sintered wicks and surface modification are mentioned below.

Zhou et al. [17] experimented with ultra-thin loop heat pipe and sintered copper mesh for cooling electronic systems. Higher capillary generation by the sintered wick was stated to be the major reason for stable operating operation of loop heat pipe at 2 W with wall temperature noted to be 43.9 °C. Also the heat pipe dissipated 12 W without any dry out occurrence. Brusly et al. [18] experimentally studied the HTP of a compact loop heat pipe using Charcoal wick and compared with the conventional copper screen mesh. The experiments were carried out from 50 to 250 W and the porosity for both the wicks was calculated as 0.63. It was reported that, the evaporator wall temperature range for charcoal wick was noted from 65 to 95 °C. The authors stated that, both the screen mesh and charcoal wick resulted in similar HTP. In addition, the charcoal wick was also suggested as a potential alternative for electronic cooling applications. Weibel et al. [19] used three different sintered porous wicks with uniform sintering, grid and radial wedge with same level porosity of 50%. Visualization study for vapor flow was carried out and observed that sintered wick created much permeable liquid paths which was stated for the reduction in thermal resistance.

Similar kind of research was carried out by Li et al. [20] by developing flattened heat pipe with three different wicks with single arch-shaped, bilateral arch-shaped and mesh–grooved type respectively. Enhancement in boiling and condensation rate of flattened heat pipe with increase in working fluid ratio was stated till dry out occurrence. In addition, Single arch-shaped wick was stated to have better HTP when compared to bilateral and mesh grooved type wicks. Also visualization study to understand the flow pattern behavior for different input heat fluxes was also presented in this work. Deng et al. [21] used four sintered wick structures (Copper wick, 123 nickel based wick, spherical shaped wick and irregular shaped wick) and compared the enhancement in capillary effect of heat pipe. Thermal imaging process was used to estimate the capillary performance of the developed sintered wicks. The particle sizes of the developed sintered wicks were 2.2–2.8, 3–7 and 75–110 μm (for spherical and irregular) respectively. It was stated that, copper wick resulted in higher capillary and permeability effect when compared with that of nickel wick. This enhancement was due to the different pore size formation for copper when compared to Nickel. Wang et al. [22] carried out an experimental work to compare the HTP of a loop heat pipe with Stainless steel and Nickel wick. Both the heat pipes are filled with R134a as working fluid. The authors stated that the higher value of pressure to temperature gradient and smaller evaporative latent heat were the most influencing factors for a better start up performance of heat pipe. In addition, antigravity experiments were also carried out to find the maximum heat transport capability of heat pipe. Wan et al. [23] used Cu/water nanofluid with sintered copper sheets inserted in the evaporator section. The use of nanofluids resulted in an average reduction of 22% in resistance value. In addition, the highest enhancement of 20% was mentioned for heat transfer coefficient at the optimum volume concentration of 1%. Wu et al. [24] used a sintered polytetrafluoroethylene (PTFE) wick to compare the HTP with nickel wick. The particle size, pore radius, porosity and permeability of PTFE wick were 300–500 μm, 1.7 μm, 50% and 6.2×10^{-12} m^2 respectively. Based on the results it was stated that, the PTFE possessed excellent wick characteristics. Moreover, the use PTFE wick resulted in reduced wall temperature of the heat pipe compared to Nickel wick, which was attributed to reduced heat accumulation and heat leak to the surroundings.

Most of the experimental works focused on heat transfer enhancement in loop heat pipe by improving the capillary effect and by increasing surface area of the evaporator section. Also, apart from the mentioned works, many research works have been published on sintered bio wicks [25–32]. However, the use of porous metal foams as a substitute of screen mesh in loop thermosyphon remains undone in the open literatures. Even though many research works have pointed out the advantages of metal foams in cooling applications, the concept of employing high thermal conductivity metal foams in thermosyphon cooling technology is still lacking and its experimental feasibility has to be discovered. Besides, a novel attempt to study the heat transfer enhancement on loop thermosyphon with metal foam inserted evaporator section for the tested heat loads (40–280 W) at vertical orientation with DI water as working fluid is carried out. In addition, the comparison of heat transfer characteristics between conventional screen wick and metal foam is presented for different filling ratio (FR = 20, 30 and 40%) with suitable heat transfer mechanisms. The idea of using metal foam to enhance the fluid's boiling rate in thermosyphon is really noteworthy in the present context.

2. Experimentation

2.1. Description of miniature loop thermosyphon

The loop thermosyphon is comprised of evaporator region, vapor/liquid tubes, condenser region, and a liquid reservoir or a compensation chamber as shown in Fig. 1. Cylindrical evaporator with 25 mm diameter and 10 mm height is fixed for entire experiments. The vapor transport line is placed vertical to ensure free flowing of vapor with relatively higher tube diameter of 6.4 mm

when compared to the liquid transport line (5.2 mm). The liquid line enters at the compensation chamber of the evaporator section to avoid reverse flow of vapor through the liquid transport line. The evaporator has an uniform wall thickness of 1 mm to ensure that the thermosyphon is capable of withstanding the operating pressure. Copper metal foam and screen wick are stacked at the individual evaporators with a compensation chamber arrangement. The total thickness of screen wick and metal foam were fixed to 4 mm due to the fabrication difficulties of metal foam. Also, the minimum fabrication thickness of metal foam is found to be 4 mm using powder metallurgy process. After inserting screen wick/metal foams in the evaporator section, the ends of every joint are perfectly brazed and the leak test is carried out to find any presence of leakage in loop thermosyphon. The compressed air up to 8 bar pressure is used to test the strength of thermosyphon to ensure safe operating condition during experiments. The total length vapor and liquid line of the loop thermosyphon is 270 mm in which the length of vapor transport, condenser and liquid transport lines are 80, 60 and 70 mm respectively. Then the loop thermosyphon is connected with the vacuum pumping system to create a vacuum pressure up to 10^{-4} mbar. Once the vacuum level is reached, DI water is filled inside the thermosyphon for a required filling ratio. The filling ratio is calculated with respected to the total volume of the thermosyphon. Then, the filling tube is tightly sealed with a crimping machine. The pressure inside the thermosyphon differs based on the input heat load from 40 to 280 W (8–57 W/cm^2) and FR for which the working pressure varies from 0.15 to 0.76 bar.

2.2. Experimental setup and procedure

The entire experimental setup required for testing the HTP of loop thermosyphon are heater, voltmeter, ammeter, cooling unit with rotameter and pump, thermocouples, data acquisition system, dimmerstat and a personal computer. The heat loss to the surrounding is reduced to the maximum level using thick layers of glass wool. Heat load is varied from 40 W to 280 W using dimmerstat and the corresponding voltage and current are measured using voltmeter and ammeter. Constant cooling water flow rate of 20 LPH is fixed for all the experimental runs. T-type thermocouples with uncertainty of ±0.5 °C are used and the temperature is measured using the data logger for every time interval of 30s. Initial phase of experiments are carried out with copper screen wick inserted thermosyphon with different FR such as 20%, 30% and 40% wherein; optimum FR (OFR) is determined. Based on the OFR, the experiments are conducted to study the HTP of metal foam inserted thermosyphon.

2.3. Preparation of metal foam

In this experimental work, compaction method is used to develop a copper metal foam with the required level of porosity (ϕ = 0.63). Commercial sugar crystals (table sugar) are used as a space holding material that can be removed either by aqueous dissolution or thermal decomposition method. The porosity of the final foam can be determined by adjusting the percentage of sugar crystals and size of the particle as per the equation in Ref. [33] which is gives as follows.

$$\frac{M_{copper}}{M_{sugar}} = \frac{\rho_{copper}}{\rho_{sugar}} \times \frac{(1-\Phi)}{\Phi} \tag{1}$$

Copper powder with 99.9% purity (particle size – 45 μm) and commercial sugar crystal with the average size distribution of 800 μm are provided as raw materials. At first step, the mixture is ball milled at 350 rpm for 2 h to ensure proper mixing of both copper powder and the sugar crystals (space holder). Then, the homogenous mixture is uni-axially compacted in a cylindrical die cavity using Universal testing machine which can exert a maximum load capacity of 100 kN. However in this work, the compression is varied from 10 kN to 25 kN from which the best foaming behavior is obtained for 20 kN. The speed of compression is constantly maintained at 0.1 mm/s whereas; the compressive load is applied on the compact for 20s for effective pressurization on the mixture. After compression, a cylindrical compact substance with 25 mm diameter and 5 mm thickness is prepared. This compressed compact is kept in the distilled water at room temperature to leach the sugar crystals. The leaching process of sugar crystals is continued for 8 h. Once the leaching process gets over, the weak compact foam is sintered at 800 °C in an electrical furnace for 4 h to impart sufficient strength. Finally, the metal foam with 63% porosity is developed by cooling the metal foam to reach the ambient temperature. The entire process involved in development of metal foam is shown in Fig. 2.

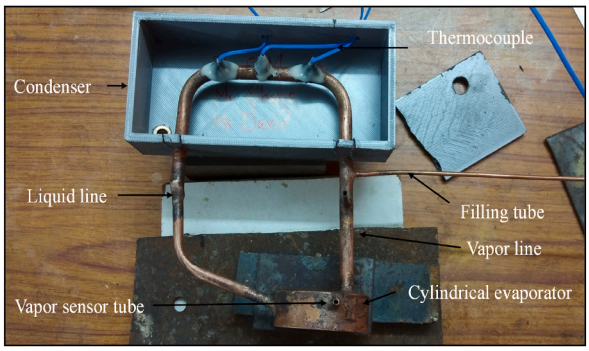

Fig. 1. Miniature loop thermosyphon.

2.4. Data reduction

The following information below deals with the calculation of derived parameters of miniature loop thermosyphon.

$$R_{thermal} = \frac{T_{evap} - T_{cond}}{Q_i} \tag{2}$$

where T_{evap} and T_{cond} represents average temperature values noted at the evaporator and condenser regions respectively.
where Q_i indicates the input heat load given on the outside wall of evaporator section

$$\text{where } Q_i = V_i \times I_i \tag{3}$$

V_i and I_i shows the voltage and current respectively.
Evaporator heat transfer coefficient (h_{evap}) is given as,

$$h_{evap} = \frac{Q_i}{A_{evap}\left(T_{evap,v} - T_{a,w}\right)} \tag{4}$$

where T_{evap} is the temperature of high pressure vapor and A_{evap} is the surface area of heat transfer.
Condenser heat transfer coefficient (h_{cond}) is given as,

$$h_{cond} = \frac{Q_{rej}}{A_{cond}\left(T_{a,w} - T_{cond,v}\right)} \tag{5}$$

where Q_{rej} is the condenser heat rejection rate and $T_{cond,v}$ is the vapor temperature of condenser.
Thermal efficiency ($\eta_{thermal}$) of thermosyphon is determined as follows.

$$\eta_{thermal} = \frac{Q_{rej}}{Q_i} \times 100 \tag{6}$$

$$Q_{rej} = m_c C_p (T_o - T_{in}) \tag{7}$$

where C_p and m_c are the specific heat and mass flow rate of cooling water.
Effective thermal conductivity (K_e) of thermosyphon is calculated as,

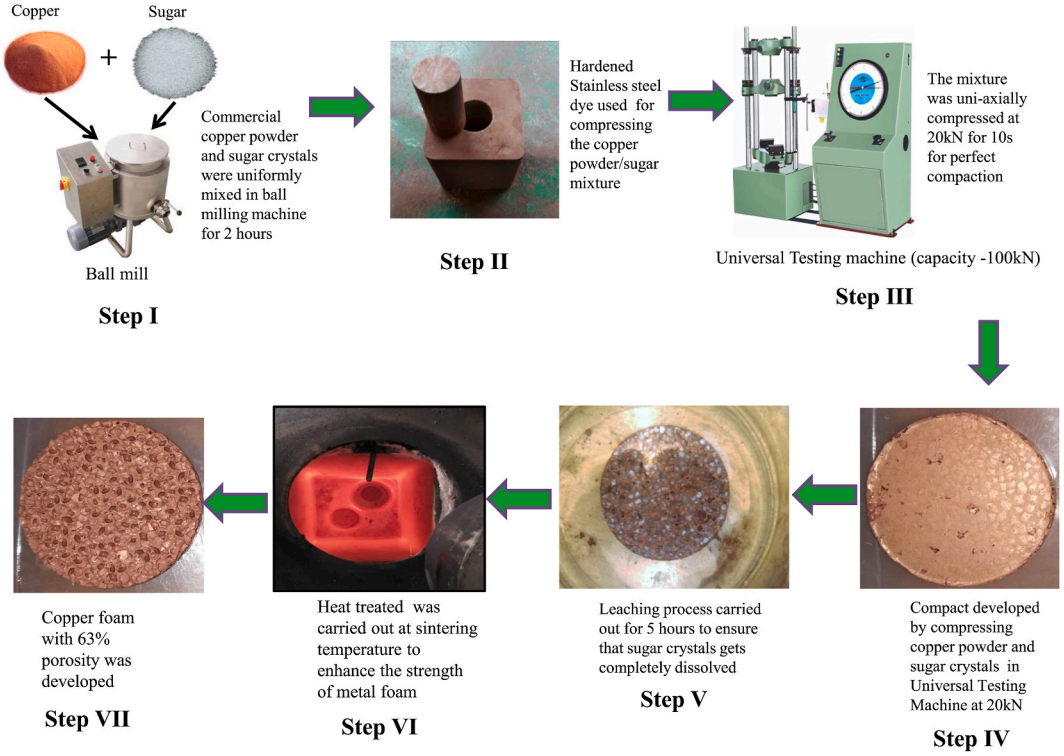

Fig. 2. Development of Copper metal foam using powder metallurgy.

$$K_e = \frac{L_e}{A_{c,area} \times R_{thermal}} \tag{8}$$

$$A_{c,area} = \frac{\pi}{4} d_o^2 \tag{9}$$

where $A_{c,area}$ is the cross-sectional area, L_e is the effective length of thermosyphon (from center of evaporator to the center of condenser) and d_o is the outer diameter of the vapor line.

Thus, the entropy due to heat transfer ($S_{g,ht}$) is calculated as mentioned in Refs. [34,35].

$$S_{g,ht} = \left(\frac{Q_i}{T_{cond}}\right) - \left(\frac{Q_i}{T_{evap}}\right) \tag{10}$$

The irreversibility due to frictional pressure drop ($S_{g,f}$) is calculated as mentioned in Refs. [34,35].

$$S_{g,f} = \frac{m_{v/l} \times \Delta p}{\rho T} \tag{11}$$

where $m_{v/l}$, is the mass flow rate.

Entropy generation due to vapor flow is given as [34],

$$S_{g,v} = \frac{8\mu_v \times Q_i^2 \times L_{v,l}}{\rho_v^2 \times h_{fg}^2 \times A_{v,l} \times T_{v\times} r_{v,l}^2} \tag{12}$$

μ_v, r_v and h_{fg} are the viscosity of vapor, radius of vapor line and latent heat respectively.

T_v and ρ_v are the vapor temperature and density corresponding to the particular heat load.

The entropy generation due to liquid flow is given as,

$$S_{g,liq} = \frac{8\mu_{liq} \times Q_i^2}{\rho_{liq}^2 \times h_{fg}^2 \times T_{liq}} \left[\frac{L_{liq,\ l1}}{A_{liq,l1} \times r_{liq,l1}^2} + \frac{L_{liq,\ l2}}{A_{liq,l2} \times r_{liq,l2}^2}\right] \tag{13}$$

The total entropy generation of thermosyphon is given as

$$S_{g,\ tot} = S_{g,ht} + S_{g,v} + S_{g,liq} \tag{14}$$

The performance of thermosyphon can be assessed by calculating the second law efficiency as given in Refs. [36–38].

$$\eta_{II} = \eta_{thermal} \left[1 - \frac{1}{\left(\frac{T_{evap,v}}{T_{evap,v} - T_{cond,v}} - 1\right)\left(\frac{T_{evap,v}}{T_s} - 1\right)}\right] \tag{15}$$

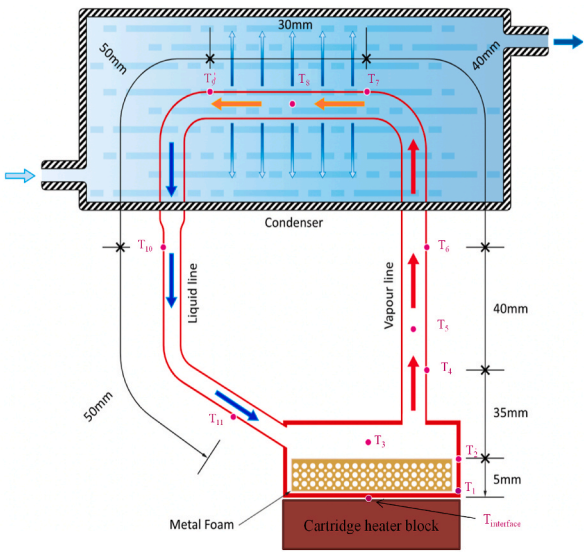

Fig. 3. Thermocouple positions on miniature loop thermosyphon.

2.5. Uncertainty analysis

The calculation of uncertainty is done mainly to deliver the correctness of the derived parameters. In this section a general procedure to calculate the uncertainty is shown in Equation (15), for a function 'R' with the independent variables x_1, x_2 …..x_n and the uncertainties associated with the independent variables y_1, y_2 ….. y_n respectively.

$$y_R = \left[\left(\frac{\partial R}{\partial x_1}y_1\right)^2 + \left(\frac{\partial R}{\partial x_2}y_2\right)^2 + \ldots + \left(\frac{\partial R}{\partial x_n}y_n\right)^2\right]^{\frac{1}{2}} \tag{16}$$

The maximum uncertainty value on Q_{in}, $R_{thermal}$, $\eta_{thermal}$, h_{evap} and $S_{g,\ ht}$ are 1.86%, 3.8%, 3.1%, 2.2% and 2.5% respectively.

3. Results and discussion

3.1. Wall temperature analysis on miniature loop thermosyphon

Fig. 3 shows the thermocouple position of miniature loop thermosyphon and the total length of 270 mm is measured from the bottom of the evaporator section to the end of the liquid line. Fig. 4(a) represents the temperature data across the length of loop thermosyphon for plain surface, screen wick and metal foam inserted conditions. The lowest wall temperature range is noticed for metal foam inserted thermosyphon for the optimum FR = 30%. The lowest wall temperature ranging from 89.4 to 54.9 °C is noted for the optimum condition when compared to screen wick thermosyphon for which the value is noted from 91.4 to 54.2 °C. The faster movement of high pressure vapor and the condensed fluid determines the lower wall temperature of a thermosyphon. Thus, for the metal foam inserted loop thermosyphon, faster rewetting of evaporator chamber occurs due to quick return of condensate. 5.1% reduction in wall temperature range is noted for metal foam filled condition. Based on the results a decreasing trend in wall temperature can be noted for metal foam filled thermosyphon at optimum FR.

In addition, experiments are conducted on miniature loop thermosyphon without a wick in the evaporator as the baseline (plain surface) only for the optimum FR of 30% and the result is shown in Fig. 4(b). Based on the results, the wickless loop thermosyphon resulted in higher evaporator wall temperature ranging from 56.8 to 97.6 °C when compared to wick and metal foam conditions (40 to 240 W). However, by increasing the heat load beyond 240 W, the evaporator wall temperature rises drastically without reaching the steady state condition which indicated its working limit. Repeatability tests are also conducted and ensured that, the maximum heat transport capacity of loop thermosyphon without wick is 240 W, whereas for screen wick and metal foam conditions it is noted as 280 W. At initial heat loads, the evaporator wall temperature of all three conditions (plain surface, screen wick and metal foam) are noted closer as the boiling and evaporation rate of the working fluid is less. Whereas for higher loads, the wall temperature is noted higher for plain surface when compared to screen wick and metal foam. This is because, the combination of higher capillary effect produced by screen wick/metal foam and the interstitial heat transfer that occurs between the metal fiber and the working fluid resulted in higher vapor generation rate [39,40] which promotes faster circulation of working fluid through the transport lines. This faster circulation makes the condensed fluid to reach the evaporator section quickly and reduces the wall temperature for metal foam/screen wick

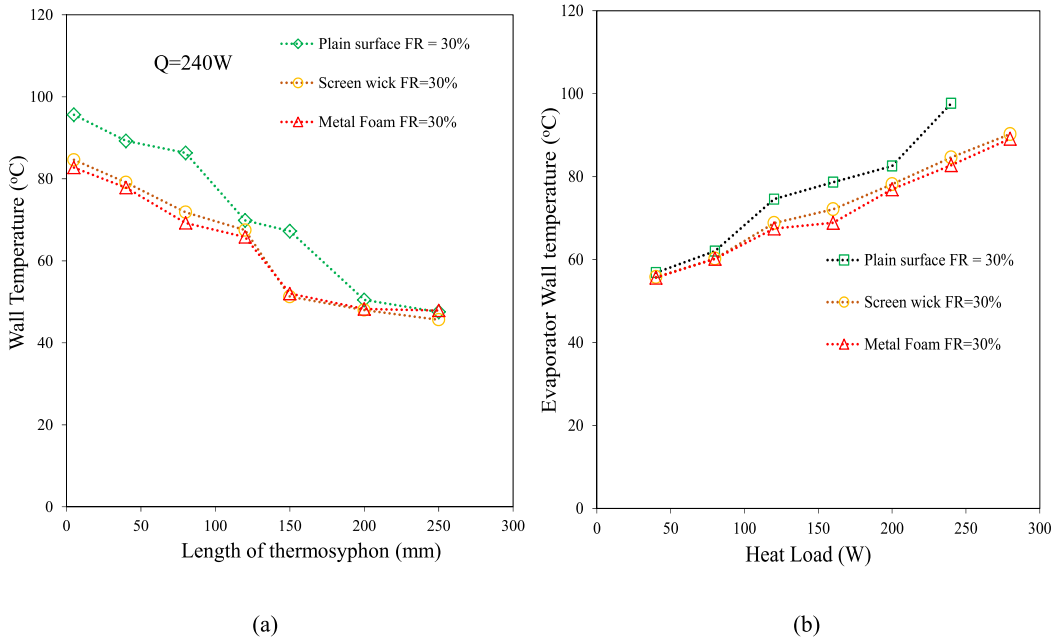

Fig. 4. (a) Variation in wall temperature across length of thermosyphon and (b) Variation in evaporator temperature for wickless, screen wick and metal foam conditions.

inserted condition when compared to the plain surface.

3.2. Evaporator wall temperature analysis and total thermal resistance of loop thermosyphon

Lowest wall temperature of a thermosyphon indicates that the condensed fluid reaches the evaporator section quickly to absorb the inner wall temperature. This happens only when the thermosyphon has optimum FR, thereby resulting in enhanced boiling and condensation rate. Fig. 5(a) shows the variation in outer wall temperature of evaporator section by comparing the screen wick and metal foam inserted thermosyphon for the tested FR (20, 30 and 40%) and heat loads (40 to 280 W). The lowest and highest wall temperature is noted for metal foam inserted thermosyphon (FR = 30%) and screen wick thermosyphon (FR=20%) respectively for all the heat load tests. The minimum wall temperature of 89.1 °C is noted with an average reduction of 5.2%. Whereas, the wall temperature of screen wick inserted thermosyphon for FR = 20% is noted to be 91.25 °C at the maximum heat load 280 W. Moreover, an increasing trend in evaporator wall temperature for all the conditions can be noted indicating the stable operating condition till 280 W. The frictional effects between the vapor and fluid are reduced as compared to conventional vertical thermosyphon due to the presence of different transport lines.

Fig. 5(b) shows the thermal resistance value of miniature loop thermosyphon for both screen wick and metal foam filled conditions. At 40 W, the thermal resistance is higher and noted to be 0.57 and 0.52 °C/W at optimum FR for screen wick and metal foam filled conditions respectively. This is because, as the boiling rate is very less at initial heat load, the sensible heating will be higher causing only lesser vapor quantity to reach the condenser. This leads to higher temperature difference resulting in higher thermal resistance. However, the thermal resistance value of metal foam filled loop thermosyphon is lesser for tested heat loads than the screen wick condition. This was due to less storage of excess heat at evaporator region. As the pore size of copper metal foam is higher when compared to screen wick, restriction of free flowing vapor between the solid fibers to the vapor transport line is very less. Whereas, this restriction phenomenon is higher for screen wick inserted mLHP, leading to higher thermal resistance. The lowest thermal resistance of 0.135 °C/W is noted for metal foam inserted thermosyphon with an average reduction of 13.8% when compared with screen wick inserted mLHP.

3.3. Variation in thermal conductivity of miniature loop thermosyphon and its efficiency

The effective thermal conductivity of miniature loop thermosyphon for screen wick and metal foam inserted conditions is shown in Fig. 6(a). As obvious, the thermal conductivity of metal foam inserted thermosyphon is higher when compared to screen wick thermosyphon. Therefore for metal foam inserted thermosyphon, as the vapor pressure is higher at the evaporator section, the vapor travels at higher velocity when compared to the metal foam thermosyphon. The highest effective thermal conductivity of 34.498 kW/mK is observed for metal foam inserted thermosyphon at the maximum heat load of 280 W. Also, an average enhancement of 9.01%, 4.8% and 8.3% are noted for metal foam inserted thermosyphon at the optimum FR of 30% when compared to FR = 20%, 30% and 40% of screen wick inserted thermosyphon respectively.(sec table 1)

Fig. 6(b) represents the variation in thermal efficiency or first law efficiency of thermosyphon for both screen wick and metal foam inserted conditions. A lesser thermal efficiency value is noted at 40 W, 5 as the single phase convection plays a major role and the vapor amount reaching the condenser region is less. Consequently, the rate of heat rejection will also be less thereby resulting in lesser thermal efficiency for all the experimental conditions. However, as the heat load is increased, the vapor quantity that reaches the condenser section to lose its latent heat will be higher causing Q_{out} value to increase. Therefore, the highest thermal efficiency of 85.13% is noted for metal foam inserted thermosyphon for the optimum FR of 30%. In addition, an average enhancement of 7.5, 3.5

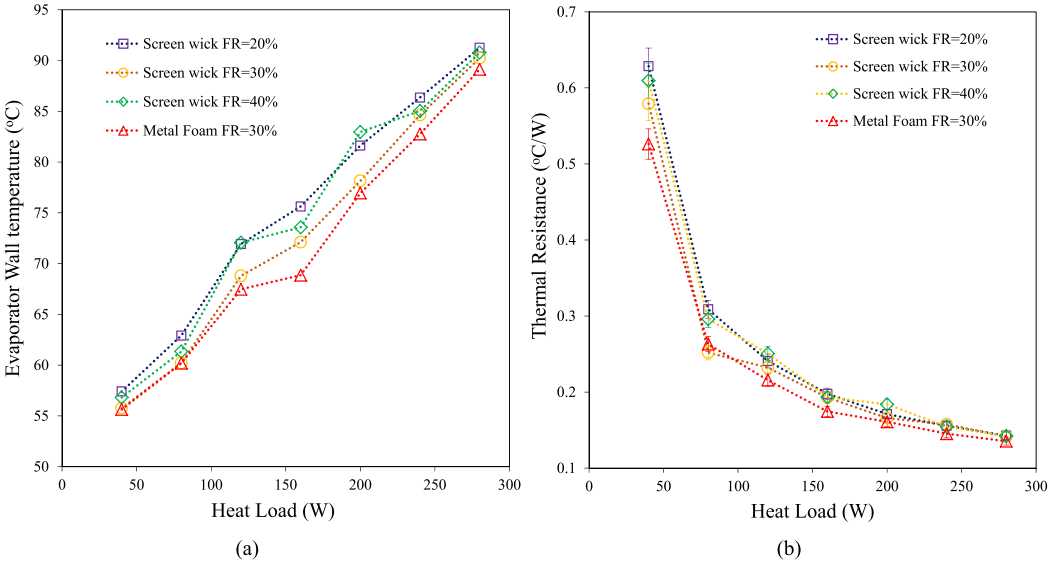

Fig. 5. Variation in (a) Evaporator wall temperature and (b) thermal resistance with respect to heat load.

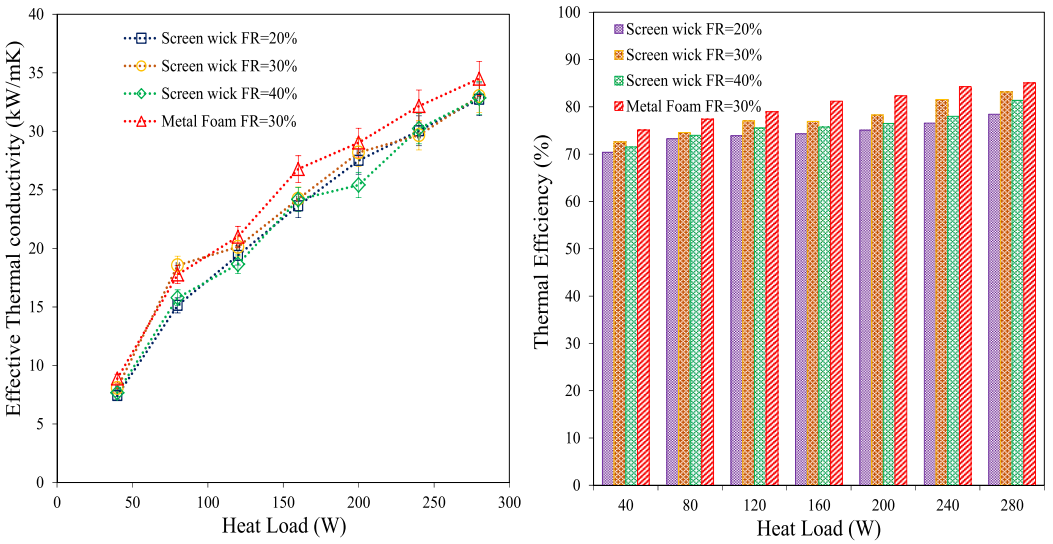

(a) (b)

Fig. 6. Variation in (a) effective thermal conductivity and (b) thermal efficiency with respect to heat load.

Table 1

Specification	Material/Dimension
Working fluid	DI water
Filling ratio (FR)	20, 30 and 40%
Heat load	40 to 280 W
mLHP	
Material	Copper
Height of evaporator	10 mm
Diameter of evaporator	25 mm
Wall thickness of evaporator	1 mm
Length of vapor line	80 mm
Length of condenser	90 mm
Length of liquid line1	25 mm
Length of liquid line2	75 mm
Diameter of vapor & liquid line1	6.4 mm
Diameter of liquid line2	5.2 mm
Condenser	
Type	Rectangular
Material	ABS plastic
Outside dimensions (lxbxh)	120 × 25 × 40 mm
Wall thickness	3 mm
Coolant	Water
Chiller temperature	18 °C
Coolant inlet temperature	20 °C
Mass flow rate	20 LPH

and 5.6% are noted for the metal foam inserted thermosyphon when compared to 20, 30 and 40% FR for screen wick thermosyphon respectively. In general, all the existing thermal system can never give 100% thermal efficiency as there will be some losses associated either due to excess heat accumulation, heat loss to surrounding, insufficient cooling etc. In this work, even though proper insulation has been ensured, there may be some loss particularly at the evaporator section. It can be noted that, the increasing rate of thermal efficiency decreases as the heat load is increased. However, an overall conclusion can be made that thermosyphon with metal foams slightly performs better when compared with conventionally used screen wicks.

3.4. Variation in heat transfer coefficient of miniature loop thermosyphon

Fig. 7(a) represents the result of evaporator heat transfer coefficient (h_{evap}) with respect to heat load for different FRs tested under vertical orientation. Based on the results, the h_{evap} value is noted increasing for all the tested heat loads. This indicates that the thermosyphon performed well without any dry out occurrence. At the initial heat loads, even though sensible heating dominates latent heat resulting in lesser vapor flow rate, the h_{evap} is noted to be higher for metal foam inserted thermosyphon when compared to screen

wick thermosyphon. The maximum h_{evap} value is noted to be 40.184 kW/m^{2}K at 280 W with the highest average enhancement of 13.17% when compared to screen wick thermosyphon filled with 20% FR. Increase in interstitial heat transfer between the fibers of metal foam and larger pore size of metal foams resulted in higher permeability when compared to screen wick thereby leading to higher h_{evap} value. In addition, the h_{evap} mainly depends on the response time of bubble nucleation and growth followed by the bubble detachment which occurs at the inner wall of the evaporator region. For an efficient working of a thermosyphon, the response time for the vaporization rate should be lesser thereby, promoting two phase heat transfer for steady state operation. Particularly, for metal foam filled thermosyphon, the interstitial heat transfer enhancement due to its higher surface-volume ratio is the major factor for the highest coefficient value.

Fig. 7(b) shows the variation in condenser heat transfer coefficient (h_{cond}) of metal foam and screen wick inserted thermosyphon for the tested heat loads (40–280 W) in vertical orientation. The process of condensation takes place when the condensation droplets are formed followed by growth and coalescence. Both conduction and convection heat transfer takes place at the condenser area wherein, the high pressure vapor rejects heat to the cooling water. Based on the results, increase in h_{cond} is noted for all the conditions. Maximum h_{cond} value of 30.63 kW/m^{2}K is noted for the metal foam filled thermosyphon at 280 W with the highest average enhancement of 18.4% when compared to screen wick thermosyphon filled with 20% FR. Further, it can be noted that the h_{cond} is almost the same for all the conditions at the initial heat load. However, the difference is observed for increase in heat loads. The lowest h_{cond} value for screen wick inserted thermosyphon is due to lesser quantity and presence of surplus fluid for 20 and 40% FR respectively which restricts the vapor to reach the condenser section respectively. Moreover, as the internal surface of condenser section remains the same for all the testing condition, the h_{cond} value directly depends mainly on the vapor generation rate of the working fluid at the evaporator section.

3.5. Variation in entropy generation in loop thermosyphon

Fig. 8(a) shows the entropy generation result between the evaporator and condenser ($S_{g,ht}$) for the tested conditions. It is well known that the entropy is defined as the measure of irreversibility. Moreover, the entropy depends mainly on the input heat flux, evaporator/condenser resistance and the surface temperature. Based on Fig. 8(a), highest $S_{g,ht}$ value is noted for screen wick inserted thermosyphon for 280 W filled with 20% FR, which confirms the higher energy loss from initial to maximum heat loads. The lowest $S_{g,ht}$ range from 0.00997 to 0.0947 W/K is noted for metal foam inserted thermosyphon at optimum FR of 30%. Also, the highest average reduction of 13.1 and 4.6% are noted for the optimum condition when compared with 20 and 30% FR of screen wick inserted thermosyphon. Reduction in entropy generation indicates that the difference between the wall temperatures and the resistance of metal foam inserted thermosyphon is very less. The larger vapor line diameter is also found to be the major reason for the reduction in entropy generation as there will be a sufficient space for the high pressure vapors to move freely in to the condenser region.

Fig. 8(b) shows the variation in entropy generation associated with pressure drop ($S_{g,\Delta p}$) of miniature loop thermosyphon for both screen wick and metal foam inserted conditions. Frictional pressure drop is one of the major influencing factors, that reduces the HTP. The entropy generation associated with frictional pressure drop is very much lesser when compared to the entropy generation associated with heat transfer. Also, an increase in entropy due to friction is noted for the tested heat loads both for screen wick and metal foam inserted thermosyphon. This can be due to the influence of vapor flow rate, density, working pressure and vapor temperature. As

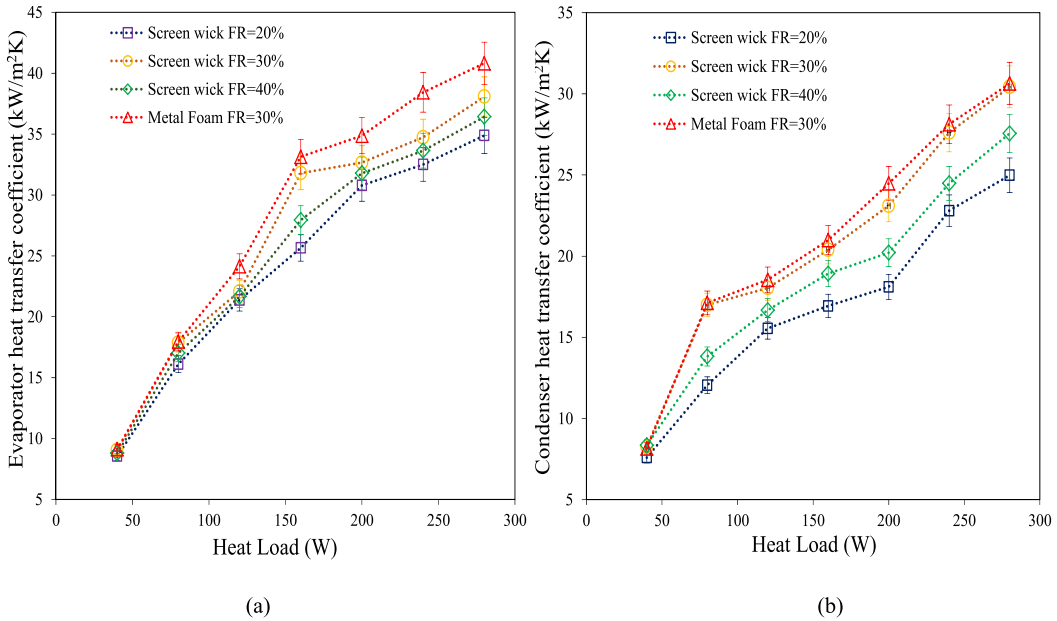

Fig. 7. Variation in (a) evaporator and (b) condenser heat transfer coefficient with respect to heat load.

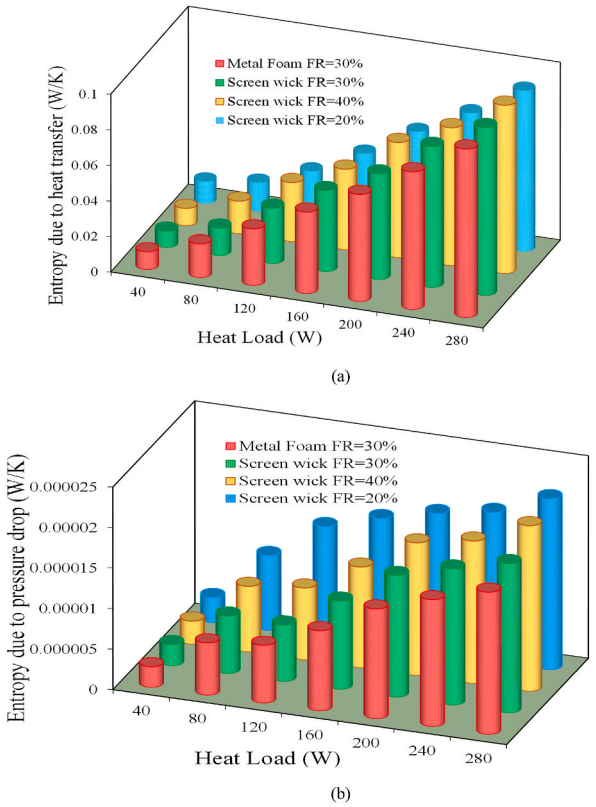

Fig. 8. Entropy generation of mLHP (a) Heat transfer between evaporator-condenser section (b) Pressure drop.

the heat load increases, both the flow rate and the pressure gradient affects the HTP of thermosyphon for both screen wick and metal foam inserted conditions. The lowest entropy value ranging from 2.5×10^{-6} to 1.7×10^{-6} W/K is noted for 30% filled metal foam inserted thermosyphon. Also an average reduction of 17.3 and 6.96% is noted for the metal foam condition when compared to 20 and 30% FR of screen wick thermosyphon respectively. In addition to vapor flow rate, working pressure and temperature, higher length of vapor and liquid line will affect the HTP of loop thermosyphon. Thus, minimizing the length of transport sections will predominantly reduce the level of entropy generation.

3.6. Variation in second law efficiency and Bejan number

Fig. 9(a) shows the results of second law efficiency of miniature loop thermosyphon for both screen wick and metal foam inserted conditions. Theoretically it can be assumed that, the adiabatic section will not lose any heat to the surrounding. However, the present thermal system resulting in cent percent efficiency with no entropy generation is practically impossible. Therefore, the thermosyphon used for this experiment is noted with entropy due to the temperature drop in the transport section. The density and viscosity variation of the working fluid is also not sufficient to dominate the entropy generation which results in heat transfer irreversibility and it reaches maximum for 280 W. As the tube diameter of vapor line is larger than the liquid line, reverse flow is eliminated which also reduces the friction between the vapor and liquid. Therefore, an average enhancement of 17.2 and 6.56% in second law efficiency are respectively noted for metal foam inserted thermosyphon when compared to 20 and 30% FR of screen wick conditions.

Fig. 9(b) shows the results of Bejan number for metal foam and screen wick inserted thermosyphon. Bejan number is the ratio of irreversibility associated with heat transfer to the pressure drop of loop thermosyphon which is shows as,

$$Be = \frac{Sg, ht}{(Sg, ht + Sg, \Delta p)} \tag{17}$$

Generally the value of Bejan number varies from 0 to 1. Be < 0.5 and Be > 0.5 shows that the irreversibility of thermosyphon is dominated by fluid friction and heat transfer respectively. In the present work, irreversibility due to heat transfer dominated for all the tested conditions. Even though the Bejan number value is lesser for screen wick inserted thermosyphon when compared to metal foam condition, it can be noted that the Bejan number ranges from 0.9994 to 0.9999 for all the experiments which shows that the entropy is dominated only by heat transfer between heat source and sink. In addition, existing literatures also state that, irreversibility due to friction will be considered negligible only when the Bejan number is closer to unity.

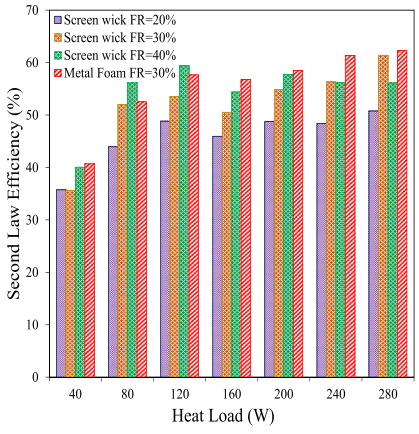

(a)

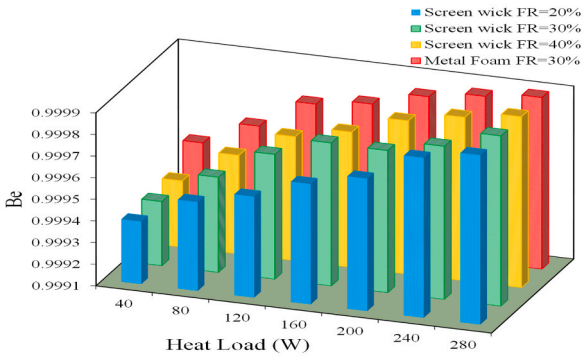

(b)

Fig. 9. (a) Variation in second law efficiency with respect to heat load (b) Variation in Bejan number with respect to heat load.

4. Conclusion

The present study deals with the experimental study on heat transfer enhancement in screen wick/metal foam inserted miniature loop thermosyphon using with DI water as working fluid for different heat loads (40–280 W) and filling ratios (FR = 20, 30 and 40%) at vertical orientation. Initial studies are carried out using thermosyphon with evaporator having copper screen wick from which the optimum FR is found (OFR = 30%). Based on the results obtained, the heat transfer study on thermosyphon with evaporator having metal foam is carried out. Interestingly, the metal foam thermosyphon outperformed screen wick thermosyphon for the OFR of 30%. An average reduction of 12.8% for total resistance and 5.2% for evaporator wall temperature respectively are noted for metal foam inserted condition with the corresponding lowest values noted as 0.135 $^{\circ}$C/W and 53.14 $^{\circ}$C. In addition the maximum h_{evap} value is noted to be 40.184 kW/m^{2}K with the average enhancement of 10.6% when compared to screen wick condition at the OFR. The heat transfer due to interstitial fibers and increased pore size of metal foam are responsible for the overall enhancement in the HTP of foam inserted thermosyphon. Also the $S_{g,ht}$ and $S_{g,\Delta p}$ values to illustrate the concept of irreversibility are also calculated in the present study. As obvious, the metal foam inserted thermosyphon performed well with the average reduction of 6.95% noted at optimum OFR when compared to screen wick conditions. Thus, the use of metal foam to enhance the fluid's boiling rate can be a better substitute for screen wick in real time engineering applications.

Credit author contribution statement

Stephen Manova: Conceptualization, Data curation, Writing – original draft. **Lazarus Godson Asirvatham:** Conceptualization, Project administration, Supervision, Writing – review & editing. **Anitha Angeline Appadurai:** Formal Analysis, Investigation. **Sheno Jerbin:** Writing – review & editing. **Jefferson Raja Bose:** Investigation. **Rajesh Nimmagadda:** Formal analysis, Data curation. **R Jayaseelan:** Data curation. **Somchai Wongwises:** Conceptualization, Investigation, Supervision.

Declaration of competing interest

The authors declare that they have no known competing financial interests or personal relationships that could have appeared to influence the work reported in this paper.

Data availability

The data that has been used is confidential.

Acknowledgement

The corresponding author acknowledges the Centre for Research in Material Sciences and Thermal Management, Karunya Institute of Technology and Sciences, Coimbatore, India for providing all the necessary facilities to conduct the experiments. The first author acknowledges the Postdoctoral Fellowship provided by King Mongkut's University of Technology Thonburi. The Eighth author acknowledges the NSTDA Research Chair Grant, and the Thailand Science Research and Innovation for the fundamental fund 2022.

Nomenclature

Q = Heat load (W)
T = Temperature (^{o}C)
R = Resistance (^{o}C/W)
V = voltage (V)
I = current (A)
h = heat transfer coefficient (W/m^2 K)
A = area (m^2)
m = mass flow rate (kg/s)
C_p = Specific heat (J/kg)
K = thermal conductivity (W/mK)
L = length (m)
S = entropy (W/K)
P = pressure (bar)
h_{fg} = latent heat of vaporization (J/kg)
r = radius (m)

Subscripts
Cu = Copper
su = sugar
evap = evaporator
cond = condenser
v = vapor
w = wall
rej = rejection
c = cooling water
o = outlet
in = inlet
e = effective
g = generation
ht = heat transfer
f = friction
l = line

Greek symbols
ϕ = porosity
Δ = difference
η = efficiency

References

[1] S. Manova, L.G. Asirvatham, R. Nimmagadda, J.R. Bose, S. Wongwises, Cooling of high heat flux electronic devices using ultra-thin multiport minichannel thermosyphon, Appl. Therm. Eng. 169 (2019) 1–23.
[2] L.G. Asirvatham, S. Wongwises, J. Babu, Heat transfer performance of a glass thermosyphon using graphene-acetone nanofluid, J. Heat Tran. 137 (11) (2015) 1–9, https://doi.org/10.1115/1.4030479.
[3] Z. Xu, Y. Zhang, B. Li, C.C. Wang, Y. Li, The influences of the inclination angle and evaporator wettability on the heat performance of a thermosyphon by simulation and experiment, Int. J. Heat Mass Tran. 116 (2018) 675–684, https://doi.org/10.1016/j.ijheatmasstransfer.2017.09.028.

[4] J.S. Chen, J.H. Chou, Cooling performance of flat plate heat pipes with different liquid filling ratios, Int. J. Heat Mass Tran. 77 (2014) 874–882, https://doi.org/10.1016/j.ijheatmasstransfer.2014.06.029.

[5] J.R. Bose, S. Manova, L.G. Asirvatham, S. Wongwises, Comprehensive case study on heat transfer enhancement using micro pore metal foams: from solar collectors to thermo electric generator applications, Case Stud. Therm. Eng. 27 (2021), https://doi.org/10.1016/j.csite.2021.101333.

[6] T.G. Karayiannis, M.M. Mahmoud, Flow boiling in microchannels: fundamentals and applications, Appl. Therm. Eng. 115 (2017) 1372–1397, https://doi.org/10.1016/j.applthermaleng.2016.08.063.

[7] A. Wlazlak, B. Zajaczkowski, M. Woluntarski, M.H. Buschmann, Influence of graphene oxide nanofluids and surfactant on thermal behaviour of the thermosyphon, J. Therm. Anal. Calorim. 136 (2) (2019) 843–855, https://doi.org/10.1007/s10973-018-7632-x.

[8] B. He, P.X. Luo, F. Yu, J. Zhou, J. Zhang, Flow boiling characteristics in bi-porous minichannel heat sink sintered with copper woven tape, Int. J. Heat Mass Tran. 158 (2020), https://doi.org/10.1016/j.ijheatmasstransfer.2020.119988.

[9] S. Manova, L. Godson Asirvatham, J. Raja Bose, T. Tharayil, S. Wongwises, Effect of confluence length on the heat transport capability of ultra-thin multiport minichannel thermosyphon, Appl. Therm. Eng. 201 (2022), https://doi.org/10.1016/j.applthermaleng.2021.117763.

[10] E.N. Stephen, L.G. Asirvatham, R. Kandasamy, B. Solomon, G.S. Kondru, Heat transfer performance of a compact loop heat pipe with alumina and silver nanofluid: a comparative study, J. Therm. Anal. Calorim. 136 (1) (2019) 211–222, https://doi.org/10.1007/s10973-018-7739-0.

[11] T. Tharayil, L.G. Asirvatham, V. Ravindran, S. Wongwises, Thermal performance of miniature loop heat pipe with graphene-water nanofluid, Int. J. Heat Mass Tran. 93 (2016) 957–968, https://doi.org/10.1016/j.ijheatmasstransfer.2015.11.011.

[12] T. Tharayil, L. Godson Asirvatham, S. Rajesh, S. Wongwises, Effect of nanoparticle coating on the performance of a miniature loop heat pipe for electronics cooling applications, J. Heat Tran. 140 (2) (2018) 1–9, https://doi.org/10.1115/1.4037541.

[13] K. Zhu, X. Chen, B. Dai, M. Zheng, Y. Wang, H. Li, Operation characteristics of a new-type loop heat pipe (LHP) with wick sepa- rated from heating surface in the evaporator, Appl. Therm. Eng. 123 (2018) 1034–1041. https://doi.org/10.1016/j.applthermaleng.2017.05.140.

[14] N. Putra, W.N. Septiadi, R. Saleh, R.A. Koestoer, S. Purbo Prakoso, The effect of CuO-water nanofluid and biomaterial wick on loop heat pipe performance, Adv. Mater. Res. 875 (877) (2014) 356–361. https://doi.org/10.4028/www.scientific.net/AMR.875-877.356.

[15] J. Liu, Y. Zhang, C. Feng, L. Liu, T. Luan, Study of copper chemical-plating modified polyacrylonitrile-based carbon fiber wick applied to compact loop heat pipe, Exp. Therm. Fluid Sci. 100 (2019) 104–113, https://doi.org/10.1016/j.expthermflusci.2018.07.008. February 2018.

[16] N. Putra, R. Saleh, W. Nata, A. Okta, Z. Hamid, International Journal of Thermal Sciences Thermal performance of biomaterial wick loop heat pipes with water-base Al 2 O 3 nano fl uids, Int. J. Therm. Sci. 76 (2014) 128–136, https://doi.org/10.1016/j.ijthermalsci.2013.08.020 [Online]. Available:.

[17] G. Zhou, J. Li, L. Lv, An ultra-thin miniature loop heat pipe cooler for mobile electronics, Appl. Therm. Eng. 109 (2016) 514–523, https://doi.org/10.1016/j.applthermaleng.2016.08.138.

[18] A.B. Solomon, A.K. Mahto, R.C. Joy, A.A. Rajan, D.A. Jayprakash, A. Dixit, A. Sahay, Application of bio-wick in compact loop heat pipe, Appl. Therm. Eng. 169 (2020), https://doi.org/10.1016/j.applthermaleng.2020.114927. July 2019.

[19] J.A. Weibel, S.V. Garimella, Visualization of vapor formation regimes during capillary-fed boiling in sintered-powder heat pipe wicks, Int. J. Heat Mass Tran. 55 (13–14) (2012) 3498–3510, https://doi.org/10.1016/j.ijheatmasstransfer.2012.03.021.

[20] J. Li, D. Wang, G.P. Peterson, Experimental studies on a high performance compact loop heat pipe with a square flat evaporator, Appl. Therm. Eng. 30 (6–7) (2010) 741–752, https://doi.org/10.1016/j.applthermaleng.2009.12.004.

[21] D. Deng, D. Liang, Y. Tang, J. Peng, X. Han, M. Pan, Evaluation of capillary performance of sintered porous wicks for loop heat pipe, Exp. Therm. Fluid Sci. 50 (2013) 1–9, https://doi.org/10.1016/j.expthermflusci.2013.04.014.

[22] H. Wang, G. Lin, L. Bai, Y. Tao, D. Wen, Comparative study of two loop heat pipes using R134a as the working fluid, Appl. Therm. Eng. 164 (2020), https://doi.org/10.1016/j.applthermaleng.2019.114459. May 2019.

[23] Z. Wan, J. Deng, B. Li, Y. Xu, X. Wang, Y. Tang, Thermal performance of a miniature loop heat pipe using water-copper nanofluid, Appl. Therm. Eng. (2018), https://doi.org/10.1016/j.applthermaleng.2014.11.010.

[24] S.C. Wu, Study of self-rewetting fluid applied to loop heat pipe, Int. J. Therm. Sci. 98 (2015) 374–380, https://doi.org/10.1016/j.ijthermalsci.2015.07.024.

[25] K.S. Yang, C.W. Tu, W.H. Zhang, C.T. Yeh, C.C. Wang, A novel oxidized composite braided wires wick structure applicable for ultra-thin flattened heat pipes, Int. Commun. Heat Mass Tran. 88 (2017) 84–90, https://doi.org/10.1016/j.icheatmasstransfer.2017.08.014.

[26] Y.F. Maydanik, S.V. Vershinin, M.A. Chernysheva, Experimental study of an ammonia loop heat pipe with a flat disk-shaped evap_orator using a bimetal wall, Appl. Therm. Eng. 126 (2017) 643–652, https://doi.org/10.1016/j.applthermaleng.2017.07.152.

[27] S. He, P. Zhou, Z. Ma, W. Deng, H. Zhang, Z. Chi, W. Liu, Z. Liu, Experimental study on transient performance of the loop heat pipe with a pouring porous wick, Appl. Therm. Eng. 164 (2020), https://doi.org/10.1016/j.applthermaleng.2019.114450. June 2019.

[28] D. Lee, C. Byon, Fabrication and characterization of pure-metal-based submillimeter-thick flexible flat heat pipe with innovative wick structures, Int. J. Heat Mass Tran. 122 (2018) 306–314, https://doi.org/10.1016/j.ijheatmasstransfer.2018.01.135.

[29] L. Jiang, J. Ling, L. Jiang, Y. Tang, Y. Li, W. Zhou, J. Gao, Thermal performance of a novel porous crack composite wick heat pipe, Energy Convers. Manag. 81 (2014) 10–18, https://doi.org/10.1016/j.enconman.2014.01.044.

[30] A.A. Abdulshaheed, P. Wang, G. Huang, C. Li, High performance copper-water heat pipes with nanoengineered evaporator sections, Int. J. Heat Mass Tran. 133 (2019) 474–486, https://doi.org/10.1016/j.ijheatmasstransfer.2018.12.114.

[31] N. Putra, W.N. Septiadi, Improvement of heat pipe performance through integration of a coral biomaterial wick structure into the heat pipe of a CPU cooling system, Heat Mass Transf. und Stoffuebertragung 53 (4) (2017) 1163–1174, https://doi.org/10.1007/s00231-016-1890-6.

[32] X. Ji, H. Li, J. Xu, Y. Huang, Integrated flat heat pipe with a porous network wick for high-heat-flux electronic devices, Exp. Therm. Fluid Sci. 85 (2017) 119–131, https://doi.org/10.1016/j.expthermflusci.2017.03.008.

[33] D.P. Mondal, H. Jain, S. Das, A.K. Jha, Stainless steel foams made through powder metallurgy route using NH4HCO3 as space holder, Mater. Des. 88 (2015) 430–437, https://doi.org/10.1016/j.matdes.2015.09.020.

[34] T. Tharayil, L.G. Asirvatham, M.J. Dau, S. Wongwises, Entropy generation analysis of a miniature loop heat pipe with graphene–water nanofluid: thermodynamics model and experimental study, Int. J. Heat Mass Tran. 106 (2017) 407–421, https://doi.org/10.1016/j.ijheatmasstransfer.2016.08.035.

[35] S. Manova, L.G. Asirvatham, R. Nimmagadda, J.R. Bose, S. Wongwises, Feasibility of using multiport minichannel as thermosyphon for cooling of miniaturized electronic devices, Heat Transf 49 (8) (2020) 4834–4856, https://doi.org/10.1002/htj.21855.

[36] T. Tharayil, L.G. Asirvatham, M.J. Dau, S. Wongwises, Entropy generation analysis of a miniature loop heat pipe with graphene–water nanofluid: thermodynamics model and experimental study, Int. J. Heat Mass Tran. 106 (2017) 407–421, https://doi.org/10.1016/j.ijheatmasstransfer.2016.08.035.

[37] L.L. Vasiliev, S.V. Konev, Thermodynamic analysis of heat pipe operation, in: Proceedings of the 7th International Heat Pipe Conference, 1990, https://doi.org/10.1016/b978-0-08-027284-9.50033-4. Minsk.

[38] H. Khalkhali, A. Faghri, Z.J. Zuo, Entropy generation in a heat pipe system, Appl. Therm. Eng. 19 (10) (1999) 1027–1043, https://doi.org/10.1016/S1359-4311(98)00089-1.

[39] S. Mancin, C. Zilio, A. Diani, L. Rossetto, Experimental air heat transfer and pressure drop through copper foams, Exp. Therm. Fluid Sci. 36 (2012) 224–232, https://doi.org/10.1016/j.expthermflusci.2011.09.016.

[40] M. Bai, J.N. Chung, Analytical and numerical prediction of heat transfer and pressure drop in open-cell metal foams, Int. J. Therm. Sci. 50 (6) (2011) 869–880, https://doi.org/10.1016/j.ijthermalsci.2011.01.007.